Engineering and Technology
2016; 3(1): 1-11
Published online January 12, 2016 (http://www.aascit.org/journal/et)
ISSN: 2381-1072 (Print); ISSN: 2381-1080 (Online)

American Association for Science and Technology

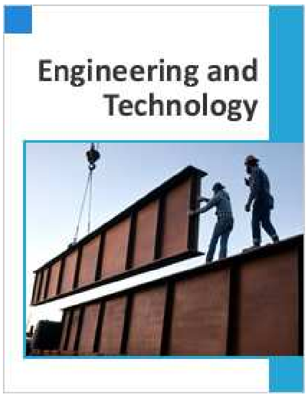

Keywords
Clamping Unit, Real-Coded Genetic Algorithm, Motor-Toggle Mechanism Two-Stage Identification

Received: December 9, 2015
Revised: December 21, 2015
Accepted: December 23, 2015

Two-Stage Identification and of a Motor-Toggle Mechanism with Clamping Effect

Yi-Lung Hsu*, Ming-Shyan Huang, Rong-Fong Fung

Department of Mechanical & Automation Engineering, National Kaohsiung First University of Science and Technology, Kaohsiung City, Taiwan

Email address
u9615907@nkfust.edu.tw (Yi-Lung H.)

Citation
Yi-Lung Hsu, Ming-Shyan Huang, Rong-Fong Fung. Two-Stage Identification and of a Motor-Toggle Mechanism with Clamping Effect. *Engineering and Technology*. Vol. 3, No. 1, 2016, pp. 1-11.

Abstract
The purpose of this study was to find two-stage identification for a motor-toggle mechanism. The effects of clamping forces on a motor-toggle mechanism are dynamically modeled in this study. The clamping unit used was a simple spring-damper model. Based on a real application, an impulse model associated with clamping effectiveness had to be considered for the process of clamping. A two-stage identification method also had to be developed to validate the dynamic responses of the unclamping and clamping motions. The two-stage identification for the system parameters was carried out through a real-coded genetic algorithm (RGA) with two different fitness functions. The purpose was to improve the accuracy of parameter identification and identify the amount of saved time, both of which were obtained by the results of numerical simulations and experimentation.

1. Introduction

Clamping force is an interesting nonlinear effect; its behavior is commonly detected in a wide variety of mechanical systems, such as injection molding machines, and has been intensively studied during the clamping motion. One fundamental characteristics of a clamping unit is unpredictable [1]. In order to obtain the high cavity pressure, when molten plastic is injected into a mold, a clamping force is applied to the clamping unit to avoid from opening [2-4]. Thus, how many of the clamping forces and the accurate position of the clamping mechanism are fundamental problems in the system identification.

One of optimization algorithm for real-coded genetic algorithm (RGA) excels at parameter identification toward the global minimum. The RGA strengths include: increasing efficiency, precision, and freedom to use different mutation and crossover methods based on the real representation [5]. In recent years, many researchers used the RGA to identify parameters for electromechanical systems [6-8]. Fung and Lin [6] applied a RGA to system identification of a plane-Type 3-DOF precision positioning table. Valarmathi et al. [7] developed a RGA method is applied to identifying the parameters of the Wiener-model in pH process. Mohideen et al. [8] proposed a simple method based on a RGA is used to tune off-line the controller parameters. The fitness function setting for the best parameter identification lies at the heart of all optimization routines. Customarily a fitness surface has many crests and trough [9]. Therefore, two-step identification approach is developed in this paper.

The main difference compared with the previous papers [10-14] is to consider the clamping unit simultaneously. The novelty of this paper include (1) develop the clamping unit model (2) the two-stage identification method for a motor-toggle mechanism in consideration with a clamping unit simultaneously, Finally, the performance between the numerical simulations and experimental results are compared for polynomials during a whole motion operation.

This paper is organized as follows. In chapter 2, the motor-toggle mechanism with a clamping effect is dynamically modeled. The stages of the one- and two-stage system identification methods are explained in chapter 3. Following that, the impulse model concerning the clamping effect of a compound clamping unit is discussed. In chapter 4, the numerical simulations and experimental results are discussed to demonstrate that the two-stage identification for the motor-toggle mechanism is indeed accuracy. Finally, conclusions are drawn in chapter 5.

2. Mathematical Model

The toggle mechanism with a clamping unit used for the electrical injection molding machine is driven by a PMSM. The experimental photo and physical model are shown in Figs. 1(a) and 1(b), respectively.

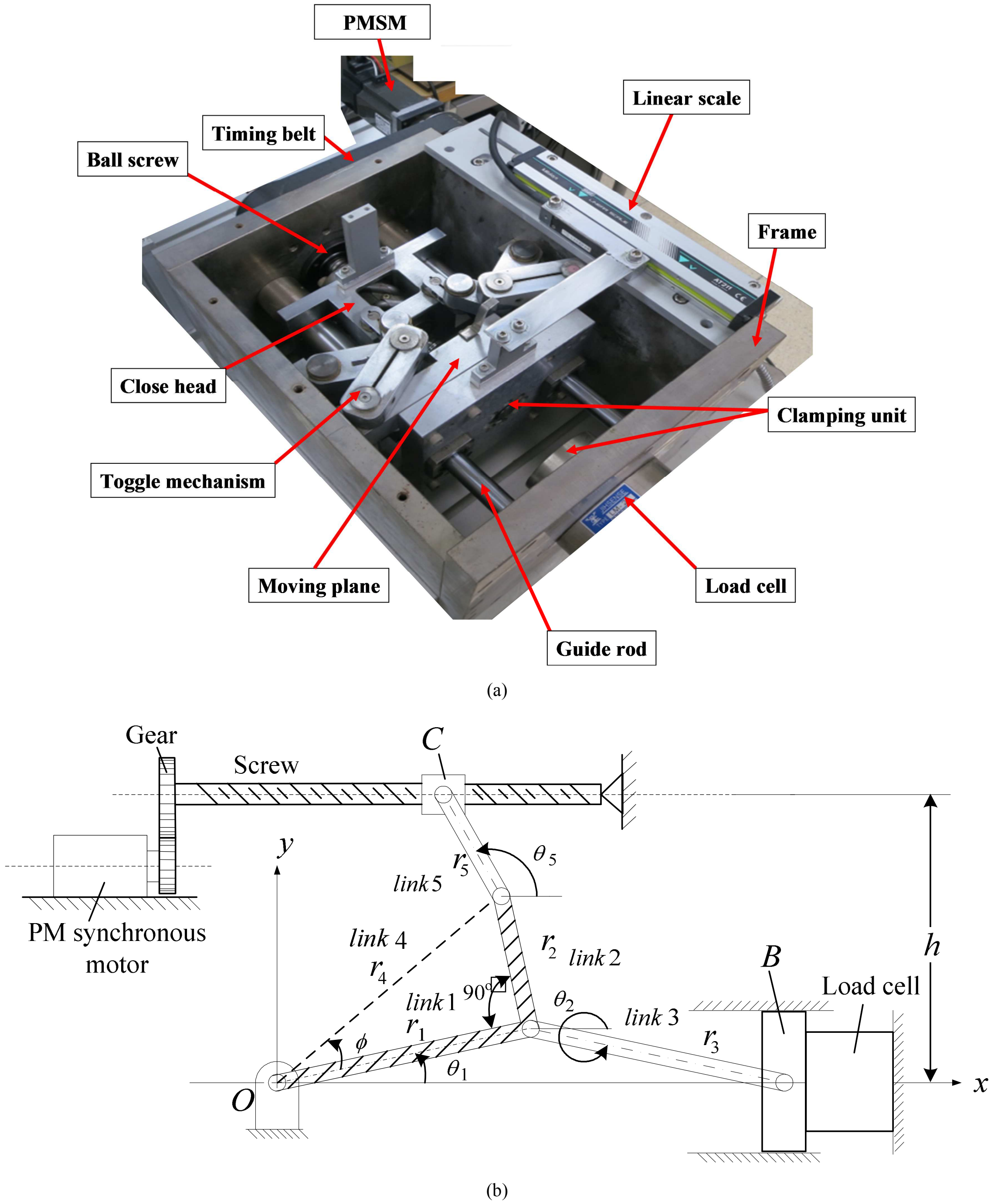

Fig. 1. A motor-toggle mechanism with clamping unit of the electrical injection molding machine. (a) The experimental equipment. (b) The physical model.

2.1. The PMSM Drive System

The electrical equation [12-13] for a PMSM is

$$L_q \frac{di_q}{dt} + R_s i_q + \omega_s \lambda_d = v_q \tag{1}$$

where L_q is the inductance, R_s is the stator resistance, ω_s and λ_d are the inverter frequency and stator flux linkage, respectively. The constant gain K_i between the PMSM and Pentium computer (PC) is assumed as

$$v_q = K_i v_{in} \tag{2}$$

where v_{in} is the control voltage from the PC.

The mechanical equation can be obtained as follows:

$$\tau_m = n(\tau_e - B_m \omega_r - J_m \dot{\omega}_r) \tag{3}$$

where τ_m is the load torque applied in the direction of angular speed ω_r, and $\dot{\omega}_r$ is the acceleration of the rotor, n is the ratio of the geared speed-reducer, B_m is the damping coefficient, and J_m is the moment of inertia. It is noted that $\omega_s = p\omega_r$, and p is the number of pole pairs. The block diagram is shown in Figs. 2.

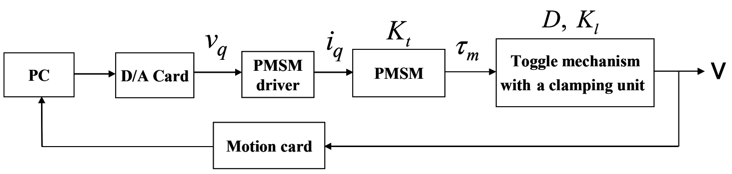

Fig. 2. *Block diagram of the motor-toggle mechanism with a clamping unit controlled by a personal computer.2.2. Impulse Model.*

This section discusses the motion in a given stroke of the motor-toggle mechanism with a clamping unit when two bodies make contact over a very short period of time during the clamping process. In general, the impact may be divided into two phases: the compression phase and the restitution phase. The former starts when the relative normal velocity is decreasing toward zero and lasts until the instantaneous common velocity of maximum compression. The latter starts at the maximum approach of the instantaneous common velocity and ends at the separation of the two colliding bodies. The impulse model approach [15] including a logical spring-damper model was employed to estimate the impact force between the two colliding bodies as follows:

$$F_i = \begin{cases} 0 & \text{if} \quad x_B < x_B^L \\ K_l z + D\dot{z} & \text{if} \quad x_B \geq x_B^L, \quad \left(z = x_B - x_B^L\right), \end{cases} \tag{4}$$

where F_i is the impulse, x_B^L is the clamping position (that is, where clamping begins), K_l is the spring parameter, z is the relative displacement or penetration between the surfaces of the two colliding bodies, $\dot{z}$ is the relative velocity, and D is the damping parameter. Figure 5 shows the impulse free body diagram of rigid body B. The damping term has different expressions depending on the conditions of the contact made, which may be valid for very elastic and/or inelastic contact. With the impulse model, the impulse occurs during the interval $t_i^- \leq t \leq t_i^+$, where t the sampled time is.

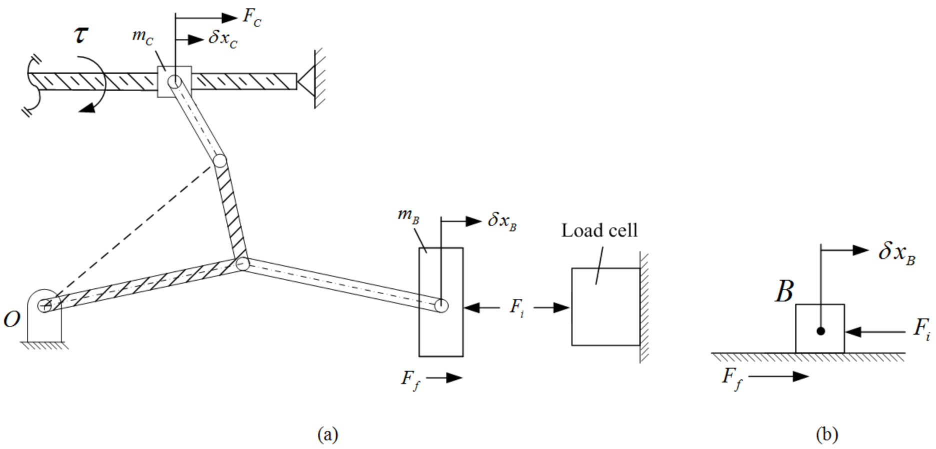

Fig. 3. *Model structure of a motor-toggle mechanism with a clamping unit. (a) Free body diagram of the contact made between slider B and load cell. (b) Impulse free body diagram of B.*

2.2. Motor-Toggle Mechanism Model

A physical model and free body diagram of the motor-toggle mechanism are shown in Fig. 1(b). The screw is the medium that converts torque τ into a force F_C that acts on slider *C*. The conversion relationship is

$$\tau = \frac{F_C L_{sd}}{2\pi n_g} \tag{5}$$

where L_{sd} is the screw lead and n_g is the gear ratio number.

The relation between slider *B* and angle θ_1 can be shown as follows:

$$x_B = 2r_1 \cos\theta_1 \tag{6}$$

$$\dot{x}_B = -2r_1\dot{\theta}_1 \sin\theta_1 \tag{7}$$

where x_B and $\dot{x}_B$ are the position and velocity of slider *B*, respectively.

Hamilton's principle and Lagrange multipliers were employed to derive the differential-algebraic equation for the motor-toggle mechanism. If force is exerted on slider *C*, links 5, 1 and 3 are driven and the output force at slider *B* increases. *h* is the height between the two horizontal guides along which sliders *B* and *C* move.

The holomonic constraint equation is

$$\Phi(\theta) = \begin{bmatrix} r_3 \sin\theta_2 + r_1 \sin\theta_1 \\ r_5 \sin\theta_5 + r_4 \sin(\theta_1 + \phi) - h \end{bmatrix} = 0, \tag{8}$$

where $\theta = \begin{bmatrix} \theta_5 & \theta_2 & \theta_1 \end{bmatrix}^{\mathrm{T}}$ is the vector of generalized coordinates, and ϕ is the angle of link 4 (see [13]). By using the principle of virtual work on the mechatronic system, it is known that virtual work will be accomplished by applied torque τ acting on the load side with a virtual angle displacement $\delta\theta$, a friction force F_f, and an impulse F_i acting on slider *B* with a virtual displacement of δx_B. Thus, the virtual work is summarized as:

$$\begin{aligned} \delta W^A &= \tau\delta\theta + (F_f - F_i)\delta x_B \\ &= F_C \delta x_C + (F_f - F_i)\delta x_B \\ &= F_C\left[-r_4 \sin(\theta_1 + \phi)\delta\theta_1 - r_5 \sin\theta_5 \delta\theta_5\right] \\ &\quad + (F_f - F_i)\left[-r_1 \sin\theta_1 \delta\theta_1 - r_3 \sin\theta_2 \delta\theta_2\right] \end{aligned} \tag{9}$$

where

$$F_C = ZK_t i_q - Z^2 J_m \ddot{x}_C - Z^2 B_m \dot{x}_C \tag{10}$$

$$Z = \frac{2\pi n_g}{L_{sd}} \tag{11}$$

$$F_f = -\mu\, m_B g \,\mathrm{sgn}(\dot{x}_B) \tag{12}$$

$$\mathrm{sgn}(\dot{x}_B) = \begin{cases} 1 & \text{if } \dot{x}_B > 0 \\ 0 & \text{if } \dot{x}_B = 0 \\ \text{-1} & \text{if } \dot{x}_B < 0 \end{cases} \tag{13}$$

μ, m_B and g are the coefficients of friction, mass of slider *B* and gravitational acceleration, respectively, x_C, $\dot{x}_C$ and $\ddot{x}_C$ are the position, velocity and acceleration of slider *C*, respectively. It should be noted that force F_C is applied to slider *C* by a PMSM relation (see [13]). The diagram of the motor-toggle mechanism with a clamping unit is shown in Fig. 3.

Equation (9) can be rewritten in the form of generalized coordinates as follows:

$$\delta W^A = -\delta\theta^{\mathrm{T}} \mathrm{Q}^{\mathrm{A}} \tag{14}$$

where

$$\delta\theta = \begin{bmatrix} \delta\theta_5 & \delta\theta_2 & \delta\theta_1 \end{bmatrix}^{\mathrm{T}}$$

$$\mathrm{Q}^{\mathrm{A}} = \begin{bmatrix} F_C r_5 \sin\theta_5 & (F_f - F_i) r_3 \sin\theta_2 & (F_f - F_i) r_1 \sin\theta_1 \\ +F_C r_4 \sin(\theta_1 + \phi) & & \end{bmatrix}$$

The generalized constraint reaction forces can be obtained in terms of Lagrange multipliers as:

$$\mathrm{Q}^{\mathrm{C}} = \Phi_\theta^{\mathrm{T}} \lambda, \tag{15}$$

where

$$\Phi_\theta = \begin{bmatrix} 0 & r_3 \cos\theta_2 & r_1 \cos\theta_1 \\ r_5 \cos\theta_5 & 0 & r_4 \cos(\theta_1 + \phi) \end{bmatrix}, \quad \lambda = \begin{bmatrix} \lambda_1 \\ \lambda_2 \end{bmatrix},$$

and λ refers to the Lagrange multipliers (see [13]). Finally, the virtual work with respect to all constraint forces is

$$\delta W^C = \delta\theta^{\mathrm{T}} \mathrm{Q}^{\mathrm{C}}, \tag{16}$$

where

$$\delta\theta^{\mathrm{T}} = \begin{bmatrix} \delta\theta_5 & \delta\theta_2 & \delta\theta_1 \end{bmatrix}^{\mathrm{T}}$$

$$\mathrm{Q}^{\mathrm{C}} = \begin{bmatrix} r_3 \cos\theta_2 \lambda_1 & r_5 \cos\theta_5 \lambda_2 & r_1 \cos\theta_1 \lambda_1 \\ +r_4 \cos(\theta_1 + \phi)\lambda_2 & & \end{bmatrix}$$

By applying the general form of Hamilton's principle,

$$
\begin{aligned}
0 &= \int_{t_1}^{t_2} \left[\delta T + \delta W^A + \delta W^C \right] dt \\
&= \int_{t_1}^{t_2} \left\{ \delta\theta^{\mathrm{T}} \left(\frac{\partial T}{\partial \theta} - \frac{d}{dt}\frac{\partial T}{\partial \dot{\theta}} + \mathrm{Q}^{\mathrm{A}} + \mathrm{Q}^{\mathrm{C}} \right) \right\} dt \\
&+ \frac{\partial T}{\partial \dot{\theta}} \delta\theta \Big|_{t_1}^{t_2},
\end{aligned}
\tag{17}
$$

where

$$T = T_2 + T_3 + T_5 + T_B + T_C,$$

from which a Euler-Lagrange equation of motion is obtained, which takes both applied and constraint forces into account, as:

$$\mathrm{M}(\theta)\ddot{\theta} + \mathrm{N}(\theta,\dot{\theta}) - \mathrm{BU} - \mathrm{D} + \Phi_\theta^{\mathrm{T}}\lambda = 0 \tag{18}$$

The matrix form can be written as:

$$\begin{bmatrix} \mathrm{M} & \Phi_\theta^{\mathrm{T}} \\ \Phi_\theta & 0 \end{bmatrix} \begin{bmatrix} \ddot{\theta} \\ \lambda \end{bmatrix} = \begin{bmatrix} \mathrm{BU} + \mathrm{D}(\theta) - \mathrm{N}(\theta,\dot{\theta}) \\ \gamma \end{bmatrix} \tag{19}$$

This is a differential-algebraic equation system. The detailed derivative and the entries of the matrices can be found in [13].

2.3. Reduced Formulation of Differential Equations of Motion

The differential-algebraic equation is summarized in matrix form. The implicit method was employed to reduce the system equations, which can be reordered and partitioned according to the decomposition of $\theta = \begin{bmatrix} \theta_5 & \theta_2 & \theta_1 \end{bmatrix}^{\mathrm{T}} = \begin{bmatrix} \mathrm{u}^{\mathrm{T}} & \mathrm{v}^{\mathrm{T}} \end{bmatrix}^{\mathrm{T}}$. If the constraints are independent, the matrix Φ_θ has full row rank, and there is always at least one non-singular sub-matrix Φ_θ of rank 3. Gauss-Jordan reduction of the matrix Φ_θ with double pivoting defines a partitioning of $\theta = \begin{bmatrix} \mathrm{u}^{\mathrm{T}} & \mathrm{v}^{\mathrm{T}} \end{bmatrix}^{\mathrm{T}}$, where $\mathrm{u} = \begin{bmatrix} \theta_5 & \theta_2 \end{bmatrix}^{\mathrm{T}}$ and $\mathrm{v} = \begin{bmatrix} \theta_1 \end{bmatrix}^{\mathrm{T}}$, such that Φ_u is the sub-matrix of Φ_θ whose columns correspond to element u of θ, and Φ_v is the sub-matrix of Φ_θ whose columns correspond to element v of θ. Thus, the matrix forms of the related equations can be written as:

$$\mathrm{M}^{\mathrm{vu}}\ddot{\mathrm{u}} + M^{\mathrm{vv}}\ddot{\mathrm{v}} + \Phi_\mathrm{v}^{\mathrm{T}}\lambda = B^{\mathrm{v}}U + D^{\mathrm{v}} - N^{\mathrm{v}} \tag{20}$$

$$\mathrm{M}^{\mathrm{uu}}\ddot{\mathrm{u}} + \mathrm{M}^{\mathrm{uv}}\ddot{\mathrm{v}} + \Phi_\mathrm{u}^{\mathrm{T}}\lambda = \mathrm{B}^{\mathrm{u}}U + \mathrm{D}^{\mathrm{u}} - \mathrm{N}^{\mathrm{u}} \tag{21}$$

$$\Phi_\mathrm{u}\ddot{\mathrm{u}} + \Phi_\mathrm{v}\ddot{\mathrm{v}} = \gamma \tag{22}$$

or in reduced form as:

$$\hat{M}(\mathrm{v})\ddot{\mathrm{v}} + \hat{N}(\mathrm{v},\dot{\mathrm{v}}) = \hat{Q}(\mathrm{v})U + \hat{D}(\mathrm{v}) \tag{23}$$

where

$$\hat{M} = M^{\mathrm{vv}} - \mathrm{M}^{\mathrm{vu}}\Phi_\mathrm{u}^{-1}\Phi_\mathrm{v} - \Phi_\mathrm{v}^{\mathrm{T}}\left(\Phi_\mathrm{u}^{-1}\right)^{\mathrm{T}}\left[\mathrm{M}^{\mathrm{uv}} - \mathrm{M}^{\mathrm{uu}}\Phi_\mathrm{u}^{-1}\Phi_\mathrm{v}\right],$$

$$\hat{N} = \left[N^{\mathrm{v}} - \Phi_\mathrm{v}^{\mathrm{T}}\left(\Phi_\mathrm{u}^{-1}\right)^{\mathrm{T}}\mathrm{N}^{\mathrm{u}}\right] + \left[\mathrm{M}^{\mathrm{vu}}\Phi_\mathrm{u}^{-1} - \Phi_\mathrm{v}^{\mathrm{T}}\left(\Phi_\mathrm{u}^{-1}\right)^{\mathrm{T}}\mathrm{M}^{\mathrm{uu}}\Phi_\mathrm{u}^{-1}\right]\gamma,$$

$$\hat{Q} = B^{\mathrm{v}} - \Phi_\mathrm{v}^{\mathrm{T}}\left(\Phi_\mathrm{u}^{-1}\right)^{\mathrm{T}}\mathrm{B}^{\mathrm{v}},\ U = i_q,\ \hat{D} = D^{\mathrm{v}} - \Phi_\mathrm{v}^{\mathrm{T}}\left(\Phi_\mathrm{u}^{-1}\right)^{\mathrm{T}}\mathrm{D}^{\mathrm{u}}.$$

The elements of the vectors u, v and matrices Φ_u, Φ_v, M^{uu}, M^{uv}, M^{vu}, M^{vv}, N^{u} and N^{v} are detailed in [13]. The resulting equation (19) is a differential equation with only one independent generalized coordinate v, which is the angle of link 1, that is, $\theta_1 = \mathrm{v}$. The system (23) becomes an initial value problem and can be integrated by using the Runge-Kutta method and the function written for ode45 in MATLAB. The electrical equation (1) for the mechatronic system can be rewritten as:

$$v_q = L_q \frac{di_q}{dt} + R_s i_q + \lambda_d \dot{\mathrm{v}} \tag{24}$$

where

$$\dot{\mathrm{v}} = -\left[\frac{L_{sd}\omega_s + \left(r_5\dot{\theta}_5 \sin\theta_5\right)}{r_4 \sin\left(\theta_1 + \phi\right)}\right]$$

v_q is the voltage command, and it drives the electric current i_q in the motor-toggle mechanism.

3. System Identification

3.1. Two-Stage Fitness Functions

The system identification procedure has a naturally logical flow: collect data, choose a fitness function, and then choose the optimal model for this system. The dynamic model of the motor-toggle mechanism with a clamping unit is modeled by Eqs. (23-24), and its parameters were identified by the RGA method. The voltage command for the system was v_q as seen in Eq. (24). In applying the RGA method, how to define the fitness function is crucial since the fitness function is a figure of merit and could be computed by using any domain knowledge.

The assigned parameters of the motor-toggle mechanism with a clamping unit used in the numerical simulations of this study are as follows: $r_1 = 0.06\ \mathrm{m}$, $r_2 = 0.032\ \mathrm{m}$, $r_3 = 0.06\ \mathrm{m}$, $r_4 = 0.068\ \mathrm{m}$, $r_5 = 0.03\ \mathrm{m}$, $h = 0.068\ \mathrm{m}$, and $\phi = 0.4899\ \mathrm{rad}$. These were substituted into in Eq. (23), and the rotation angle and speed were calculated by the Runge-Kutta numerical method. In system identification, the real-coded genetic algorithm method is employed to find optimal parameters. The parameter identification can be carried out in one-stage and two-stage processes.

3.1.1. One-Stage Identification

In this study, one- and two-stage identification methods were proposed and compared. The advantage of the one-stage identification method is that it can identify all parameters of the motor-toggle mechanism with a clamping unit simultaneously. However, its drawback is that identifying all the parameters is time-consuming. In order to identify all parameters $(B_m,\ D,\ J_m,\ K_i,\ K_l,\ K_t,\ L_q,\ R_s,\ m_2,\ m_3,\ m_5,\ m_B,\ m_c,\ \mu$ and $\lambda_d)$ of the mechatronic system, the fitness function was designed as follows:

$$F_1\left(15 \text{ parameters}\right) = 1 / \sum_{j=1}^{n} E_j^{\ 2} \tag{25}$$

$$E_j = \mathrm{v}^{(j)} - \mathrm{v}^{*(j)} \tag{26}$$

where n is the total number of sampled time intervals, E_j is the calculated error at the j^{th} sampled time interval, $\mathrm{v}^{(j)}$ is the experimental angular displacement at the j^{th} sampled time interval, and $\mathrm{v}^{*(j)}$ is the solution found through the Runge-Kutta method to solve Eqs. (23-24) with the identified parameters from the RGA method.

3.1.2. Two-Stage Identification

For the two-stage identification method, the unclamping parameters of the mechanical and electrical equations can be identified in the first stage (from the initial position to the position just before the clamping process takes place). The clamping parameters D and K_l can be found in the second stage during the clamping interval. The two-stage identification method has the advantage of saving on computation time in different stages, and it is more accurate. However, its drawback is that the fitness functions need to be defined for the two different stages.

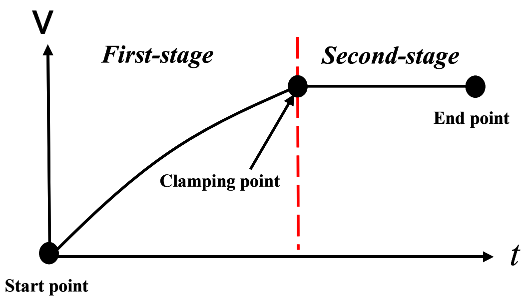

Fig. 4. Scheme of the two-stage identification method for the motor-toggle mechanism with a clamping unit.

A. First-stage identification

For the first stage of identification, the fitness function was designed as follows:

$$F_F\left(13 \text{ parameters}\right) = 1 / \sum_{j=1}^{n} E_{1j}^2 \tag{27}$$

$$E_{1j} = \mathrm{v}^{(j)} - \mathrm{v}^{*(j)} \tag{28}$$

where the 13 parameters of $B_m,\ J_m,\ K_i,\ K_t,\ L_q,\ R_s,\ m_2,\ m_3,\ m_5,\ m_B,\ m_c,\ \mu$ and λ_d were identified, n is the total number of sampled time intervals and E_{1j} is the calculated error at the j^{th} sampled time interval. The time sampled was from the initial position to the position just before clamping.

B. Second-stage identification

The second stage of identification was used for clamping parameters D and K_l during the clamping interval. The model of the impulse is described by Eq. (4). The fitness function was designed as follows:

$$F_S\left(D,\ K_l\right) = 1 / \sum_{j=1}^{n} E_{2j}^2 \tag{29}$$

$$E_{2j} = \mathrm{v}^{(j)} - \mathrm{v}^{*(j)} \tag{30}$$

where n is the total number of sampled time intervals and E_{2j} is the calculated error at the j^{th} sampled time interval. The other notations are identical to those found in Eqs. (25-26).

3.2. RGA

In this study, the RGA was applied to identify the system parameters. The RGA is an optimization searching algorithm which simulates a mechanism of evolution on a computer-based platform in conjunction with natural selection and genetic principles. The chromosomes are expressed by vectors, and each element of the vectors is called a gene. The initial real-valued genes in the chromosomes are obtained by generating a sequence of real-valued variables from a randomly limited range. All the chromosomes form a population and are evaluated according to the pre-given evaluation index and given fitness values. Chromosome reproduction, crossover and mutation are carried out in accordance with fitness values. The chromosomes with lower fitness values are discarded, and the chromosomes with higher fitness values kept. Those kept form a new population, which may be better than the old population. The RGA continuously searches for better chromosomes in this way until the converging index is satisfied. The procedure of the RGA is discussed in [16], and the detailed method for RGA parameter identification of the system is found in [13]. In the following sections about identification of the system parameters, the design of the fitness function and the employment of the RGA identification method are discussed.

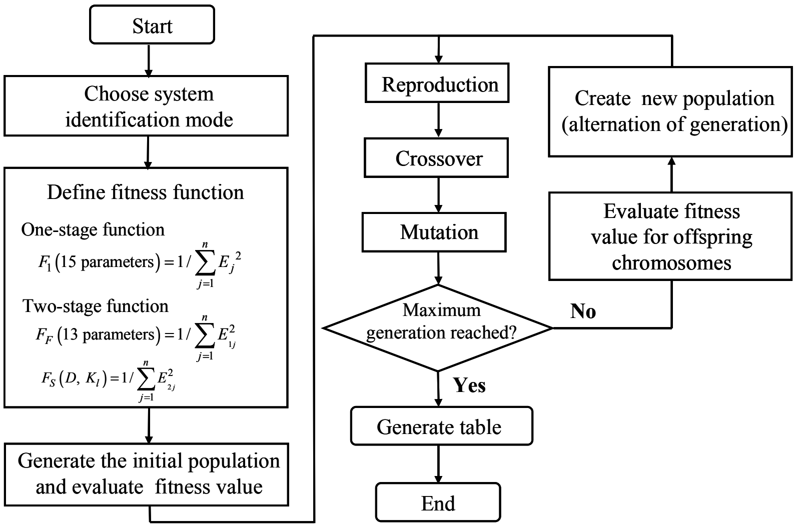

Fig. 5. Flow chart for two-stage system identification based on RGA method.

3.3. Swept-Frequency Sinusoid Waveform

In system identification for parameters, the dynamic model of electrical and mechanical equations is utilized to identify the motor-toggle mechanism with a clamping unit based on the RGA. Here, a swept-frequency sinusoid waveform of the applied voltage command [17] was adopted as follows:

$$v_q(t) = A + B\sin\left[\omega(t) \operatorname{mod}(t,\ T)\right] \tag{31}$$

$$\omega(t) = \omega_0 + (\omega_1 - \omega_0) \operatorname{mod}\left(\frac{t}{T},\ 1\right) \tag{32}$$

where A and B are the bias and amplitude of the voltage command v_q, respectively. ω_0 and ω_1 represent the minimum and maximum frequencies, respectively. T is the period, and *mod* denotes the modulus after division, respectively. The advantage of the swept-frequency sinusoid waveform system identification method is that it can simulate the mechanical properties of a motor-toggle mechanism with a clamping unit simultaneously. The voltage command v_q of Eq. (31) was used to excite the motor-toggle mechanism with a clamping unit.

4. Numerical Simulations and Experimental Results

4.1. Experimental Setup

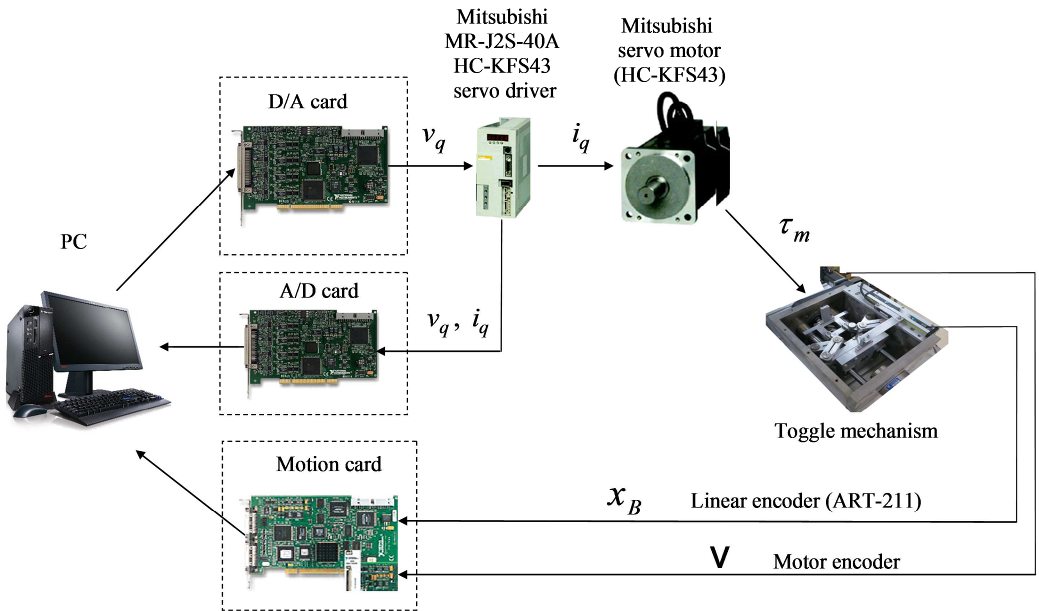

Fig. 6. Experimental setup block diagram of the motor-toggle mechanism.

The experimental setup for the toggle mechanism with a clamping unit driven by a PMSM is shown in Fig. 6. The PMSM was driven by a MITSUBISHI HC-KFS13 series. The specifications are shown as follows: rated torque of 1.3 Nm, rated output of 400 W, rated rotational speed of 3,000 rpm and rated current of 2.3 A. The waveform of the input voltage was generated by LabVIEW, which is a Windows-supported graphical programming language. The linear encoder (Mitutoyo AT211) used had a high-response speed of 2 m/sec (at 1 μm resolution). The displacement signal was transformed via an A/D converter card. Finally, the experimental results from the response signals were analyzed. A D/A converter (NI PCI-6733E) with a resolution of 12 bits were used to transform the voltage waveform to the MITSUBISHI HC-KFS13 series of the PMSM drive. The control system used was a sine-wave PWM control, which is a voltage control system. The way to find the displacement produced by the PMSM is to measure the voltage from the linear encoder sensor.

4.2. Numerical Simulation Results

For numerical simulation, the system of Eqs. (23-24) was identified. In the RGA the crossover probability was 0.7, the mutation probability was 0.05, the population size was 1,000, and the maximum generation number was 100. The clamping position x_B started at 56 mm. The computation times for the one- and two-stage methods were about 50 and 40 minutes, respectively.

Figure 7(a) shows the evolution histories of fitness value for the one- and two-stage RGA methods. The respective fitness values were 1,090,865 and 1,226,344 for the one- and two-stage identification methods, and they converged at the 62nd and 52nd generations, respectively. Figure 7(b) shows the swept-frequency sinusoid waveform of the voltage command with the values of A =0.05, B = 0.01, ω_0 = 0.5, ω_1 = 40 and T = 5.

Figure 7(b-h) show the related data for the one- and two-stage identification methods by using the swept-frequency sinusoid waveform voltage command. It can be seen that the displacement in Fig. 7(c) and the impulse in Fig. 7(d) for the three values are almost the same. Figs. 7(e-h) show that the errors of one- and two-stage identification methods with respect to the assigned parameters are very slight.

In conclusion regarding numerical identification for the motor-toggle mechanism with a clamping unit, the results produced by the two-stage identification method are closer to the assigned parameters than those of the one-stage identification method.

In order to validate the feasibility of the proposed RGA method, the assigned parameters and the identified results of the one- and two-stage methods are shown in Table 1. Their errors were compared, and it was found that the two-stage identification results were better than those of one-stage identification. Moreover, the two-stage results approached the assigned parameters with errors of less than 2%.

Table 1. *Comparisons of identified parameters for the assigned parameters, one- and two-stage methods in numerical simulations.*

Parameters	**Feasible domains**	**Assigned (A)**	**One-stage (B)**	**% error |A-B|/A. %**	**Two-stage First-stage (C)**	**Two-stage Second-stage (C)**	**% error |A-C|/A. %**
B_m (Nms/rad)	0-1	0.0112	0.0124	10.71%	0.01137	-	1.52%
D (Ns/m)	$0-1\times10^6$	15,000	16,400	9.33%	-	15,300	2.00%
J_m (Nms^2)	0-0.001	6.70×10^{-5}	6.155×10^{-5}	8.13%	6.770×10^{-5}	-	1.04%
K_i	$0-1\times10^4$	1.00×10^2	1.11×10^2	11.0%	1.015×10^2	-	1.50%
K_l (N/m)	$0-1\times10^8$	5.0×10^7	4.486×10^7	10.28%	-	4.92×10^7	1.60%
K_t (Nm/A)	0-10	0.5087	0.5743	12.90%	0.5031	-	1.10%
L_q (H)	0-0.01	2.1×10^{-3}	2.291×10^{-3}	9.1%	2.132×10^{-3}	-	1.52%
R_s (Ω)	0-1	1.406×10^{-2}	1.279×10^{-2}	9.03%	1.379×10^{-2}	-	1.92%
m_2 (kg)	0-10	1.610	1.706	5.96%	1.606	-	0.25%
m_3 (kg)	0-10	1.820	1.611	11.47%	1.829	-	0.49%
m_5 (kg)	0-10	0.950	0.852	10.28%	0.932	-	1.86%
m_B (kg)	0-10	4.000	4.374	9.35%	4.074	-	1.85%
m_C (kg)	0-10	3.000	3.250	8.33%	3.051	-	1.68%
μ	0-10	0.170	0.162	4.82%	0.168	-	1.29%
λ_d	0-1	0.036	0.039	8.33%	0.0366	-	1.67%

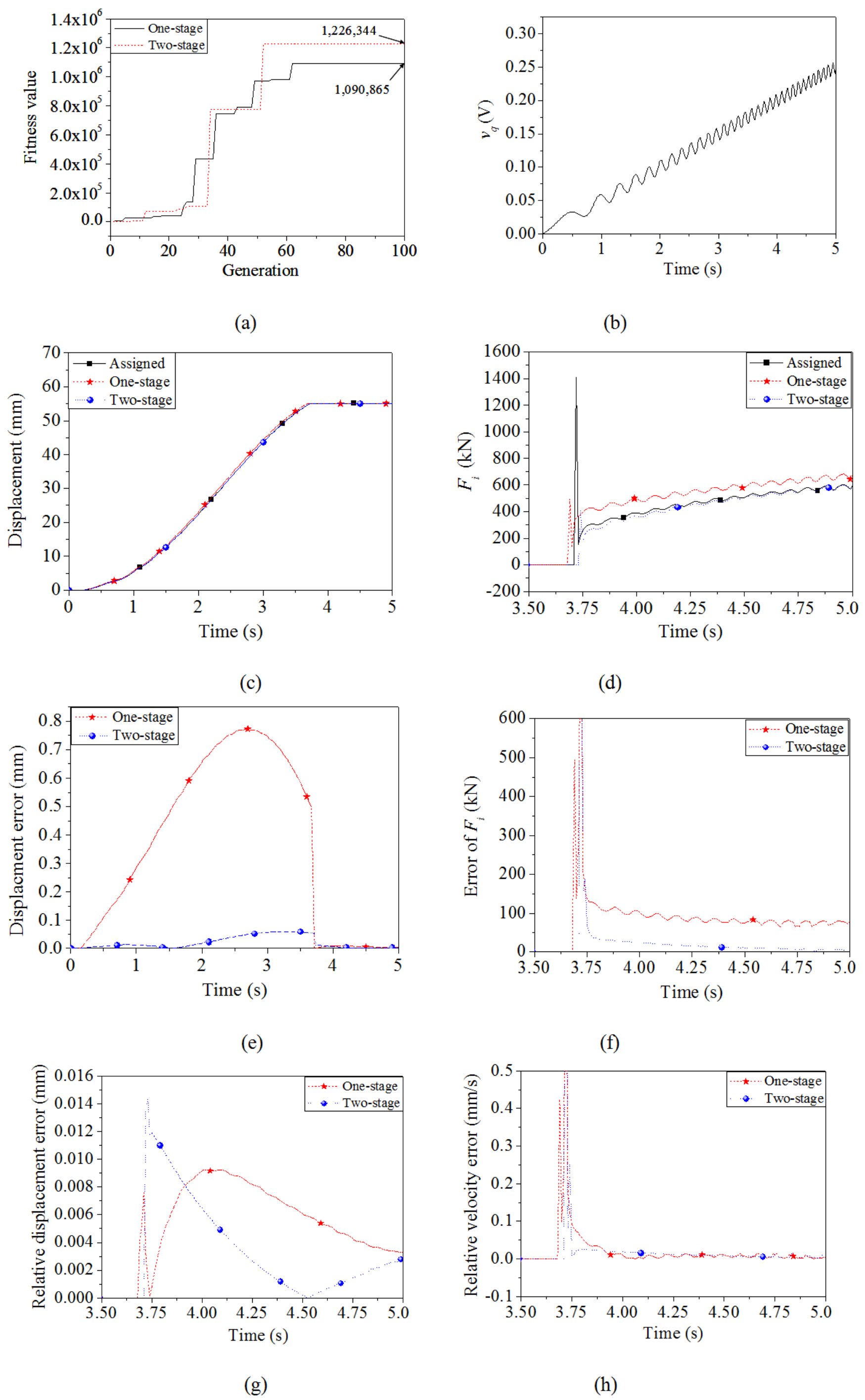

Fig. 7. *Comparisons of assigned parameters, one-stage and two-stage dynamic responses by the voltage command swept-frequency sinusoid waveform of the motor-toggle mechanism with a clamping unit. (a) Evolution histories of assigned identified parameters. (b) Voltage command. (c) Displacement. (d) Impulse. (e) Displacement error. (f) Impulse error. (g) Relative displacement error. (h) Relative velocity error.*

4.3. Experimental Results

The swept-frequency sinusoid waveform of the voltage command with the values of A =0.25, B = 0.01, ω_0 = 0.5, ω_1 = 40 and T = 5 were also used in the experimental identification. The sampled time interval was 0.001 s, and the total time measured was 5 s. The RGA notation and setting were the same as those of the numerical simulations. Using fitness functions (25), (27) and (29), the identified parameters of the motor-toggle mechanism with a clamping unit system and the relative errors of the one-stage parameters with respect to the two-stage method are shown in Table 2. The computation times for the one- and two-stage methods were about 54 and 41 minutes, respectively. The respective final fitness values of the one- and two-stage identification methods were about 797,624 and 928,182, and they converged at the 69th and 61st generations, respectively.

Moreover, these parameters were employed in Eqs. (23-24) to simulate dynamic responses of the motor-toggle mechanism. Figure 8 compares the dynamic responses of the experimental, one- and two-stage identified displacements x_B. The final positions were at about 56.521 mm, 56.865 mm and 56.657 mm, and the final displacement errors were about 0.344 mm and 0.136 mm. In conclusion regarding experimental identification, it was found that the results of the two-stage identification were very close to those of the real system.

The experimental results show that the proposed two-stage identification method can improve the accuracy of parameter identification by 11% and can save 24% on time compared to the one-stage identification method. The results have been obtained through verification.

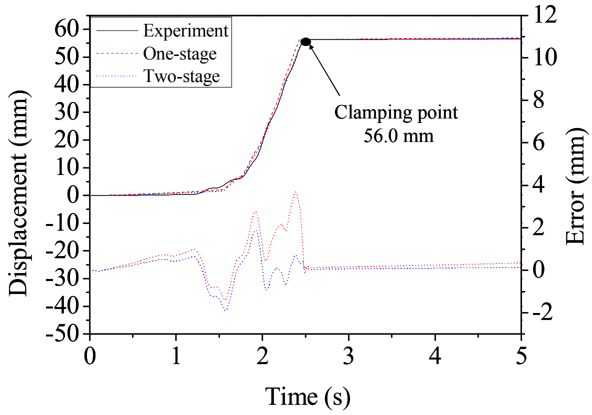

Fig. 8. *Comparisons of experimental, one-stage and two-stage dynamic responses with voltage command swept-frequency sinusoid waveform of the toggle mechanism.*

Table 2. *Experimentally identified parameters of the motor-toggle mechanism.*

Parameters	One-stage / Two-stage (A) (B)	% error |B-A|/B. %
B_m (Nms/rad)	0.0122 / 0.0112	8.93%
D (Ns/m)	980 / 1,100	10.91%
J_m (Nms^2)	6.393×10^{-5} / 6.7×10^{-5}	4.58%
K_i	1.26×10^{2} / 1.15×10^{2}	9.57%
K_l (N/m)	1.080×10^{7} / 0.993×10^{7}	8.76%
K_t (Nm/A)	0.6141 / 0.5652	8.65%
L_q (H)	2.357×10^{-3} / 2.158×10^{-3}	9.22%
R_s (Ω)	1.305×10^{-2} / 1.424×10^{-2}	8.36%
m_2 (kg)	1.758 / 1.615	8.85%
m_3 (kg)	1.995 / 1.822	9.5%
m_5 (kg)	1.220 / 1.296	5.86%
m_B (kg)	6.471 / 7.125	9.18%
m_C (kg)	4.956 / 5.460	9.23%
μ	0.585 / 0.647	9.58%
λ_d	0.034 / 0.037	8.11%

4.4. Discussion

This study provides a much more detailed exploration of system identification for a motor-toggle mechanism with a clamping unit compared to previous studies, being enhanced by using a dynamical model of the impulse model. The one- and two-stage identification methods of the RGA were employed to identify the new modeling system parameters during the clamping process. In order to obtain more accurate parameters, a two-stage identification method was found to be necessary as shown by comparisons of both numerical simulation results and experimental results, which make it obvious, that the two-stage identification method performs better than the one-stage method. Finally, this procedure can also be applied to any mechatronic system with a clamping unit, for example, intelligent machine tool systems used in forming, cutting, or the joining of diagnostic procedure subsystems.

5. Conclusions

In this paper, enhances the previous studies' findings by providing a much more detailed research of system identification for a toggle mechanism with clamping unit driven by a PMSM. By comparing this paper with former studies, we summarize this paper with the following results, that is, (1) the proposed two-stage identification of RGA is applied to identifying the parameters of the clamping-model in clamping process. Also computing the optimal value of stiffness parameter of clamping unit has been analyzed. (2) That two main qualities described the clamping model: simplicity and reliability. Similar procedure can be applied to any mechatronic system with a clamping unit.

Acknowledgement

The financial support from the Ministry of Science and

Technology of the Republic of China with contract number MOST 103-2221-E-327-009-MY3 is gratefully acknowledged.

References

[1] Oyetunji A. Development of small injection molding machine for forming small plastic articles for small-scale industries. Journal of Engineering Science and Technology 2010; 5(1): 17–29.

[2] Sun SH. Optimum topology design for the stationary platen of a plastic injection machine. Computers in Industry 2004; 55(2): 147–158.

[3] Chakherlou TN, Abazadeh B, Vogwell J. The effect of bolt clamping force on the fracture strength and the stress intensity factor of a plate containing a fastener hole with edge cracks. Engineering Failure Analysis 2009; 16: 242–253.

[4] Huang MS, Lin TY, Fung RF. Key design parameters and optimal design of a five-point double-toggle clamping mechanism. Applied Mathematical Modelling 2011; 35: 4304–4320.

[5] Wright AH. Genetic algorithms for real parameter optimization. First Workshop on the Foundations of Genetic Algorithms and Classier Systems. Morgan Kaufmann Publishers. Los Altos A 1991; 205–218.

[6] Fung RF, Lin WC. System identification and contour tracking of a plane-type 3-DOF (X,Y,θ_z) precision positioning table. IEEE Transactions on Control Systems Technology 2010; 18(1): 22–34.

[7] Valarmathi K, Devaraj D, Radhakrishnan TK. Real-coded genetic algorithm for system identification and controller tuning. Applied Mathematical Modelling 2009; 33(8): 3392–3401.

[8] Mohideen KA, Saravanakumar G, Valarmathi K, Devaraj D, Radhakrishnan TK. Real-coded genetic algorithm for system identification and tuning of a modified model reference adaptive controller for a hybrid tank system. Applied Mathematical Modelling 2013; 37(6): 3829–3847.

[9] Tohsato Y, Ikuta K, Shionoya A, Mazaki Y, Ito M. Parameter optimization and sensitivity analysis for large kinetic models using a real-coded genetic algorithm. Gene 2013; 518(1): 84–90.

[10] Lin FJ, Fung RF, Wai RJ. Comparison of sliding mode and fuzzy neural network control for motor-toggle servomechanism. IEEE/ASME Transactions on Mechatronics 1998; 3(4): 302–318.

[11] Engleder S. Time-optimal motion planning and control of an electrohydraulically actuated toggle mechanism. Mechatronics 2007; 17: 448-456.

[12] Huang MS, Chen KY, Fung RF. Numerical and experimental identifications of a motor-toggle mechanism, Applied Mathematical Modeling 2009; 33(5): 2502–2517.

[13] Hsu YL, Huang MS. Fung RF. System identification of a motor-toggle mechanism with clamping effect. The 3rd International Conference on Engineering and Technology Innovation (ICETI 2014), Kenting, Taiwan, November 1–2, 2014.

[14] Hsu YL, Huang MS. Fung RF. Adaptive tracking control of a motor-toggle mechanism with clamping effect. Proceedings of 6th International Conference on Positioning Technology (ICPT 2014), Kitakyushu, Japan, November 18–21, 2014.

[15] Khulief YA, Shabana AA., A Continuous force model for the impact analysis of flexible multibody systems. Mechanism and Machine Theory 1987; 22(3): 213–224.

[16] Haupt RL, Haupt SE. Practical genetic algorithms, 2nd Edition, John Wiley & Sons, New Jersey. 2004

[17] Fuh CC. Tsai HH. Adaptive parameter identification of servo control systems with noise and high-frequency uncertainties. Mechanical Systems and Signal Processing 2007; 21: 1437-1451.